The Astrophysical Journal Letters, 849:L15 (6pp), 2017 November 1 https://doi.org/10.3847/2041-8213/aa9372

On the Effects of Pickup Ion-driven Waves on the Diffusion Tensor of Low-energy Electrons in the Heliosphere

N. Eugene Engelbrecht
Center for Space Research, North-West University, Potchefstroom, 2522, South Africa; n.eugene.engelbrecht@gmail.com
Received 2017 September 29; revised 2017 October 12; accepted 2017 October 12; published 2017 October 26

Abstract

The effects of Alfvén cyclotron waves generated due to the formation in the outer heliosphere of pickup ions on the transport coefficients of low-energy electrons is investigated here. To this end, parallel mean free path (MFP) expressions are derived from quasilinear theory, employing the damping model of dynamical turbulence. These are then used as inputs for existing expressions for the perpendicular MFP and turbulence-reduced drift coefficient. Using outputs generated by a two-component turbulence transport model, the resulting diffusion coefficients are compared with those derived using a more typically assumed turbulence spectral form, which neglects the effects of pickup ion-generated waves. It is found that the inclusion of pickup ion effects greatly leads to considerable reductions in the parallel and perpendicular MFPs of 1–10 MeV electrons beyond ∼10 au, which are argued to have significant consequences for studies of the transport of these particles.

Key words: cosmic rays – diffusion – Sun: heliosphere – turbulence

1. Introduction

From theoretical (see, e.g., Lee & Ip 1987; Williams & Zank 1994; Zank 1999; Isenberg 2005), observational (e.g., Joyce et al. 2010; Cannon et al. 2014a, 2014b, 2017; Aggarwal et al. 2016), and numerical (Hellinger & Trávníček 2016) studies we now know that the continual production of pickup protons from incoming interstellar neutral hydrogen by means of photoionization or charge exchange with solar wind protons (see, e.g., Scherer et al. 2014) leads to the formation of Alfvén cyclotron waves that in turn lead to an enhancement in the wave frequency spectra at large frequencies. In situ observations of such enhancements have, however, only rarely been seen (e.g., Cannon et al. 2014a). All current detections are, however, limited to within 6 au, within or at the edge of the ionization cavity (Cannon et al. 2017), which is variously estimated to extend to between 4 and 8 au (see, e.g., Smith et al. 2001; Isenberg 2005; Isenberg et al. 2010; Schwadron & McComas 2010). Furthermore, Cannon et al. (2017) note that, for their data, the turbulence is only rarely weak enough to render the excited waves observable. Beyond the distances these authors consider, however, the background turbulence levels are expected to decrease considerably, a decrease accompanied by an increase in the pickup ion contribution (see, e.g., Weygand et al. 2016; Wiengarten et al. 2016; Zank et al. 2017). The mechanism whereby solar wind protons are heated due to the turbulent decay of these fluctuations has been very successfully invoked in the models of, e.g., Smith et al. (2001), Breech et al. (2008, 2009), and Isenberg et al. (2010) so as to reproduce the observed non-adiabatic radial profile of the solar wind proton temperature observed by the *Voyager* spacecraft (Richardson et al. 1995).

To date, not much attention has been given to the influence that these fluctuations may have on the transport of charged energetic particles. Williams & Zank (1994) showed that the spectral contribution due to these fluctuations should extend, in the outer heliosphere at least, from wavenumbers equal to Ω/v_p to Ω/v_A, where Ω denotes the proton gyrofrequency, and v_A and v_p the Alfvén and pickup ion (PUI) speeds, respectively. Assuming a Parker (1958) heliospheric magnetic field (HMF), a radial density profile that goes as r^{-2} (normalized to a value of 7 particles per cm^3 at Earth), and that v_p is approximately twice the solar wind speed, this range of wavenumbers corresponds roughly to that which, in the quasilinear theory (QLT) formulation of Jokipii (1966), would effectively pitch-angle scatter electrons with energies of ∼1–10 MeV parallel to the background HMF (see also Bieber et al. 1994; Giacalone & Jokipii 1999). Given the proximity of Jupiter to the edge of the ionization cavity, the fact that it is a powerful source of low-energy electrons in precisely this energy range (see, e.g., Simpson et al. 1974; Eraker 1982), and that the transport of these Jovian electrons, as well as that of low-energy galactic electrons, has been demonstrated to be extremely sensitive to changes in their diffusion coefficients (e.g., Ferreira et al. 2001a, 2001b; Engelbrecht & Burger 2010, 2013b), the present study undertakes to theoretically take into account the effect of PUI-generated waves on the diffusion tensor of such electrons. This is done by deriving an appropriate QLT expression for the parallel mean free path (MFP) employing the damping model of dynamical turbulence (see, e.g., Bieber et al. 1994), following the approach outlined by Teufel & Schlickeiser (2003). The QLT has several limitations (see, e.g., Shalchi 2009 and references therein), but provides a reasonably tractable point of departure when one attempts to describe the parallel diffusion of charged particles (e.g., Bieber et al. 1994). This result is then used as an input value for a reasonable analytical approximation to the nonlinear guiding center (NLGC) theory (originally proposed by Matthaeus et al. 2003) perpendicular MFP expression derived by Shalchi et al. (2004), which in turn is used as an input for a turbulence-reduced drift coefficient proposed by Engelbrecht et al. (2017). Although more advanced theories exist from which the perpendicular MFP may be calculated (see, e.g., Shalchi 2010), the NLGC approach provides a simple, tractable expression that has been employed in previous electron transport studies (e.g., Engelbrecht & Burger 2010). This approach requires an estimation of how much fluctuation energy at a given position is due to these waves. To this end, a two-component turbulence transport model (TTM) is employed, that of Oughton et al. (2011). The two-component wavelike/quasi-2D formalism is advantageous to this study, as the wave energy due to the formation of PUIs is assigned to the correct component (Hunana & Zank 2010). Although a more advanced incarnation of this model exists, namely, that of Wiengarten et al. (2016), the Oughton et al. (2011) model yields the same results in the region of the heliosphere dominated by the supersonic solar wind, which is the region of interest to this study.

2. Coefficients

The QLT MFP parallel to the background HMF B_o is given by (e.g., Jokipii 1966; Earl 1974)

$$\lambda_\parallel = \frac{3v}{8}\int_{-1}^{1}\frac{(1-\mu^2)^2}{D_{\mu\mu}(\mu)}d\mu, \quad (1)$$

where v denotes the particle speed, μ the cosine of the particle pitch angle, and $D_{\mu\mu}(\mu)$ the pitch-angle Fokker–Planck coefficient. This last quantity, employing the damping model of dynamical turbulence, is given by Teufel & Schlickeiser (2003) as

$$D_{\mu\mu}(\mu) = \frac{2\pi\Omega^2(1-\mu^2)}{B_o^2}\int_0^\infty g_{sl}(k_\parallel)q_D f(k_\parallel)dk_\parallel, \quad (2)$$

with

$$f(k_\parallel) = \frac{1}{1+q_D^2(k_\parallel v_\parallel+\Omega)^2} + \frac{1}{1+q_D^2(k_\parallel v_\parallel-\Omega)^2}. \quad (3)$$

Note that $q_D = (\alpha v_A|k_\parallel|)^{-1}$, with $\alpha \in [0, 1]$ as a parameter governing the strength of dynamical effects, is set to 1 for the rest of this study. The quantity $g_{sl}(k_\parallel)$ denotes the one-sided slab fluctuation spectrum. This spectrum is considered to be the sum of the spectrum due to the PUI contribution g_{pi} and a background spectrum g_b so that $g_{sl}(k_\parallel) = g_{pi}(k_\parallel) + g_b(k_\parallel)$. From Equation (2) then this would imply that $D_{\mu\mu}(\mu) = D_{\mu\mu}^b + D_{\mu\mu}^{pi}$. The background spectrum is modeled following Teufel & Schlickeiser (2003) so as to consist of a wavenumber-independent energy-containing range, a Kolmogorov inertial range, and a dissipation range with spectral index $-p$:

$$g_b(k_\parallel) = \begin{cases} g_o k_m^{-s}, & |k_\parallel| \leqslant k_m; \\ g_o|k_\parallel|^{-s}, & k_m \leqslant |k_\parallel| \leqslant k_d; \\ g_1|k_\parallel|^{-p}, & |k_\parallel| \geqslant k_d. \end{cases} \quad (4)$$

The quantities k_m and k_D denote the wavenumbers at which the inertial and dissipation ranges commence, respectively, while $g_1 = g_0 k_d^{p-s}$ and

$$g_o = \left[s + \frac{s-p}{p-1}\left(\frac{k_m}{k_d}\right)^{s-1}\right]^{-1}\frac{\delta B_{sl}^2 k_m^{s-1}(s-1)}{8\pi}, \quad (5)$$

with δB_{sl}^2 denoting the total variance of the slab fluctuations without the PUI-generated component, and $s = 5/3$. Note that $1 < s < 2$. If the PUI-generated component were to be completely neglected, use of Equations (2) and (4) would lead to the solutions for $\lambda_\parallel$ presented for various parameter ranges by Teufel & Schlickeiser (2003). Engelbrecht & Burger (2013b) present an expression for $\lambda_\parallel$ constructed from the abovementioned damping turbulence solutions, given by

$$\lambda_\parallel = \frac{3s}{\sqrt{\pi}(s-1)}\frac{R^2}{k_{\min}}\left(\frac{B_o}{\delta B_{\rm slab}}\right)^2[\lambda_e + \lambda_i + \lambda_d], \quad (6)$$

$$\begin{aligned} \lambda_e &= \frac{1}{4\sqrt{\pi}}, \\ \lambda_i &= \frac{2R^{-s}}{\sqrt{\pi}(2-s)(4-s)}, \\ \lambda_d &= {}_2F_1\left(1, \frac{1}{p-1}, \frac{p}{p-1}; -\frac{\pi a}{f_1}Q^{p-2}\right)\frac{\sqrt{\pi}a}{f_1 R^s Q^{p-s}}, \end{aligned} \quad (7)$$

where $a = v/(\alpha v_A)$, $f_1 = 2(p-s)/(p-2)(2-s)$, $R = R_L k_{\min}$, $Q = R_L k_d$, and R_L is the maximal Larmor radius. The spectral contribution due to PUI-generated waves is modeled following the wavenumber dependence of the theoretical result of Williams & Zank (1994) for an azimuthal background field (a valid assumption beyond the ionization cavity), and is given by

$$g_{pi}(k_\parallel) = \begin{cases} \frac{g_3}{k_\parallel^2}\left(v_p - \frac{\Omega}{k_\parallel}\right), & \Omega/v_p \leqslant k_\parallel \leqslant \Omega/v_A; \\ 0, & \text{for all other } k_\parallel, \end{cases} \quad (8)$$

where $g_3 = 2\Omega\delta B_{pi}^2/(v_A - v_p)^2$ is a normalization constant so that the integral over g_{pi} to wavenumber $k_\parallel$ is equal to the variance δB_{pi}^2 due to PUI-generated fluctuations alone.

Using the full spectrum $g_{pi} + g_b$ in Equation (2) to evaluate $D_{\mu\mu}$ results in an intractable integral. Therefore, it is assumed that g_{pi} dominates over the wavenumber range where it assumes non-zero values, so that for electrons with wavenumbers resonating in this range, $D_{\mu\mu}(\mu) \approx D_{\mu\mu}^{pi}$. Then Equation (2) can be rewritten as

$$D_{\mu\mu}(\mu) = \frac{4\pi(1-\mu^2)\delta B_{pi}^2}{R_L^3 B_o^2}\frac{v^2}{(v_A - v_p)^2}(I_1(\mu) - I_2(\mu)), \quad (9)$$

where

$$\begin{aligned} I_1(\mu) &= v_p R_L^2\int_{x_1}^{x_2} x\left[\frac{1}{1+a^2(\mu+x)^2} + \frac{1}{1+a^2(\mu-x)^2}\right], \\ I_2(\mu) &= \Omega R_L^3\int_{x_1}^{x_2} x^2\left[\frac{1}{1+a^2(\mu+x)^2} + \frac{1}{1+a^2(\mu-x)^2}\right], \end{aligned}$$

with $x = (R_L k_\parallel)^{-1}$, $x_2 = v_p/\Omega R_L$ and $x_1 = v_A/\Omega R_L$. Integration then yields

$$\begin{aligned} I_1(\mu) = \frac{1}{2a^2}\log&\left[\frac{(h_{2,-}^2+1)(h_{2,+}^2+1)}{(h_{1,-}^2+1)(h_{1,+}^2+1)}\right] \\ &+ \frac{\mu}{a}(\tan^{-1}(h_{1,+}) - \tan^{-1}(h_{1,-}) \\ &+ \tan^{-1}(h_{2,-}) - \tan^{-1}(h_{2,+})) \end{aligned}$$

and

$$I_2(\mu) = \frac{2}{a^2}(x_2 - x_1) + \frac{\mu}{a^2}\log\left[\frac{(h_{2,-}^2 + 1)(h_{1,+}^2 + 1)}{(h_{1,-}^2 + 1)(h_{2,+}^2 + 1)}\right] + \frac{1 - a^2\mu^2}{a^3}(\tan^{-1}(h_{1,+}) + \tan^{-1}(h_{1,-}) - \tan^{-1}(h_{2,-}) - \tan^{-1}(h_{2,+})),$$

where, for convenience of notation, $h_{i,\pm} = a(x_i \pm \mu)$ with $i = 1$, 2. To analyze Equation (9), some measure of the turbulence conditions in the outer heliosphere is required. To this end, the Oughton et al. (2011) TTM is solved in the solar ecliptic plane for generic solar minimum conditions, exactly as was described by Engelbrecht & Burger (2013a) for a scenario where the PUI source term is active, and when PUI driving is completely neglected. The difference in wavelike fluctuation energies thus calculated in the outer heliosphere (with PUI effects minus without) would then provide a very rough estimation of δB_{pi}^2, which can then be employed to evaluate Equation (9). Note that in what is to follow the outputs of the non-PUI-driven TTM will be used as inputs for the background turbulence spectral form $g_b(k_\|)$ (Equation (4)) and all quantities calculated from it, so as to remain as self-consistent as possible.

These outputs, for the wavelike quantities, are shown in the top and middle panels of Figure 1 as a function of heliocentric radial distance. Solutions without PUI driving are shown in red, those including this effect in blue. Note that quasi-2D quantities are not shown here. The interested reader is referred to Engelbrecht & Burger (2013a, 2015) for a discussion of them. Beyond ∼5 au the effects of PUI driving become readily apparent, with the difference in wavelike energies between these solutions growing to more than two orders of magnitude at 100 au. The correlation scales diverge similarly. As an example, the 1 MeV pitch-angle Fokker–Planck diffusion coefficient calculated using Equation (9) is shown in the very bottom panel of Figure 1 as a function of the cosine of the pitch angle. Note that a logarithmic scale is employed in the y-axis of this figure, so as to make it clear that this coefficient does not assume zero values for particles with 90° pitch angles, as expected from the assumption of dynamical turbulence (e.g., Schlickeiser 2002; Shalchi 2009). The form of $D_{\mu\mu}$ here is dominated by the $1 - \mu^2$ term in Equation (2) close to $\mu = \pm 1$ and assuming zero values at 0° and 180° pitch angle, although this is masked by the logarithmic scale used in the figure. To derive a parallel MFP expression using Equation (9), one must integrate Equation (1) numerically. The results of this integration, shown as a function of rigidity at various radial distances, can be seen in the left panels of Figure 2, corresponding to energies below ∼10 MeV, along with the corresponding damping turbulence MFPs (Equation (6)) calculated assuming no PUI driving and a dissipation range onset frequency equal to the proton gyrofrequency (Leamon et al. 2000). These results are shown for maximum dynamical effects ($\alpha = 1$) and reduced dynamical effects ($\alpha = 0.1$). The small rigidity range for the PUI-affected solutions corresponds to the range over which $D_{\mu\mu}$ would be dominated by the PUI-driven fluctuation spectrum g_{pi}. For the relevant rigidities and both values for α, the differences between solutions with and

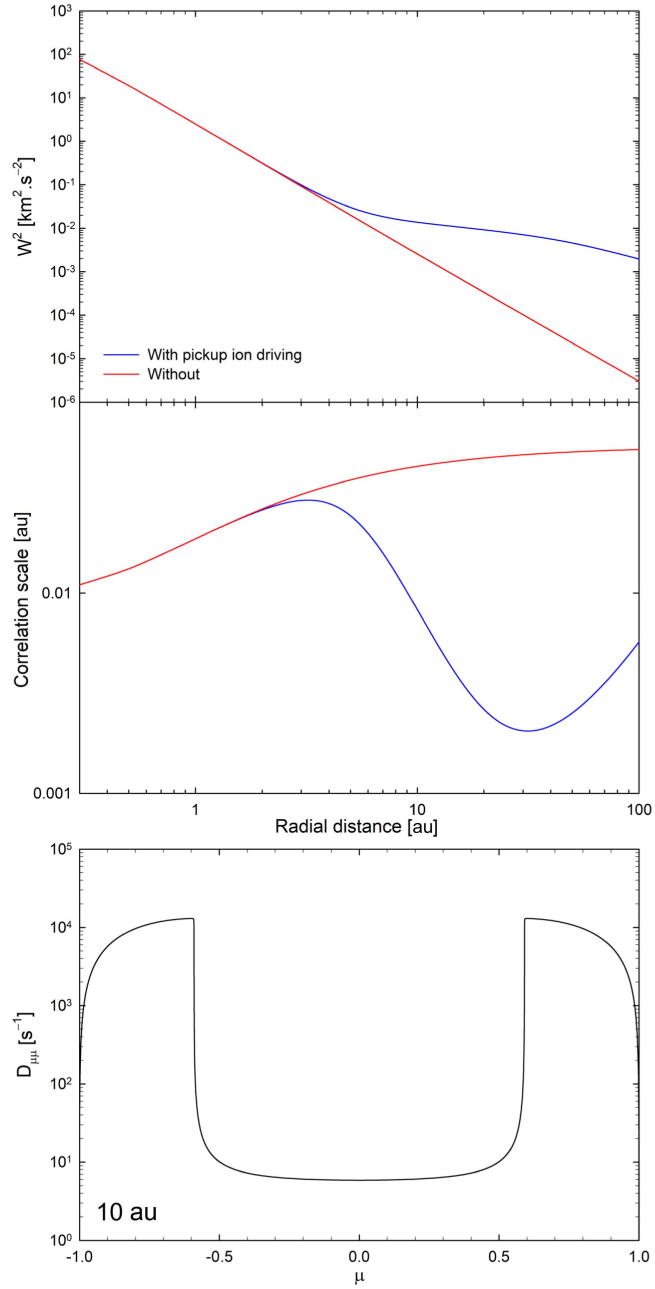

Figure 1. Wavelike energies (top panel) and parallel correlation scales (middle panel) yielded by the Oughton et al. (2011) TTM model both with (blue lines) and without (red lines) PUI driving. Bottom panel shows $D_{\mu\mu}$ (Equation (9)) at 1 MeV as function of μ at 10 au using inputs from the abovementioned TTM.

without PUI-driven waves are very large. This is not entirely surprising, as from Figure 1 it is clear that an extraordinary amount of power would go to spectrum g_{pi} relative to g_b, and from the increases in the low-rigidity parallel MFPs when PUI effects are ignored. The MFPs derived assuming PUI effects are essentially constant as a function of rigidity, as expected from Equation (9) and the rigidity dependences of I_1 and I_2, and do not vary much with radial distance. Reducing dynamical effects by a factor of 10 leads to an increase in both sets of parallel MFPs, which is roughly an order of magnitude for the PUI-influenced results. To get an estimate of the behavior of the perpendicular MFP, the results for $\lambda_\|$ are used as inputs for the NLGC expression employed by Burger et al. (2008), which is a modification of the result presented by Shalchi et al. (2004)

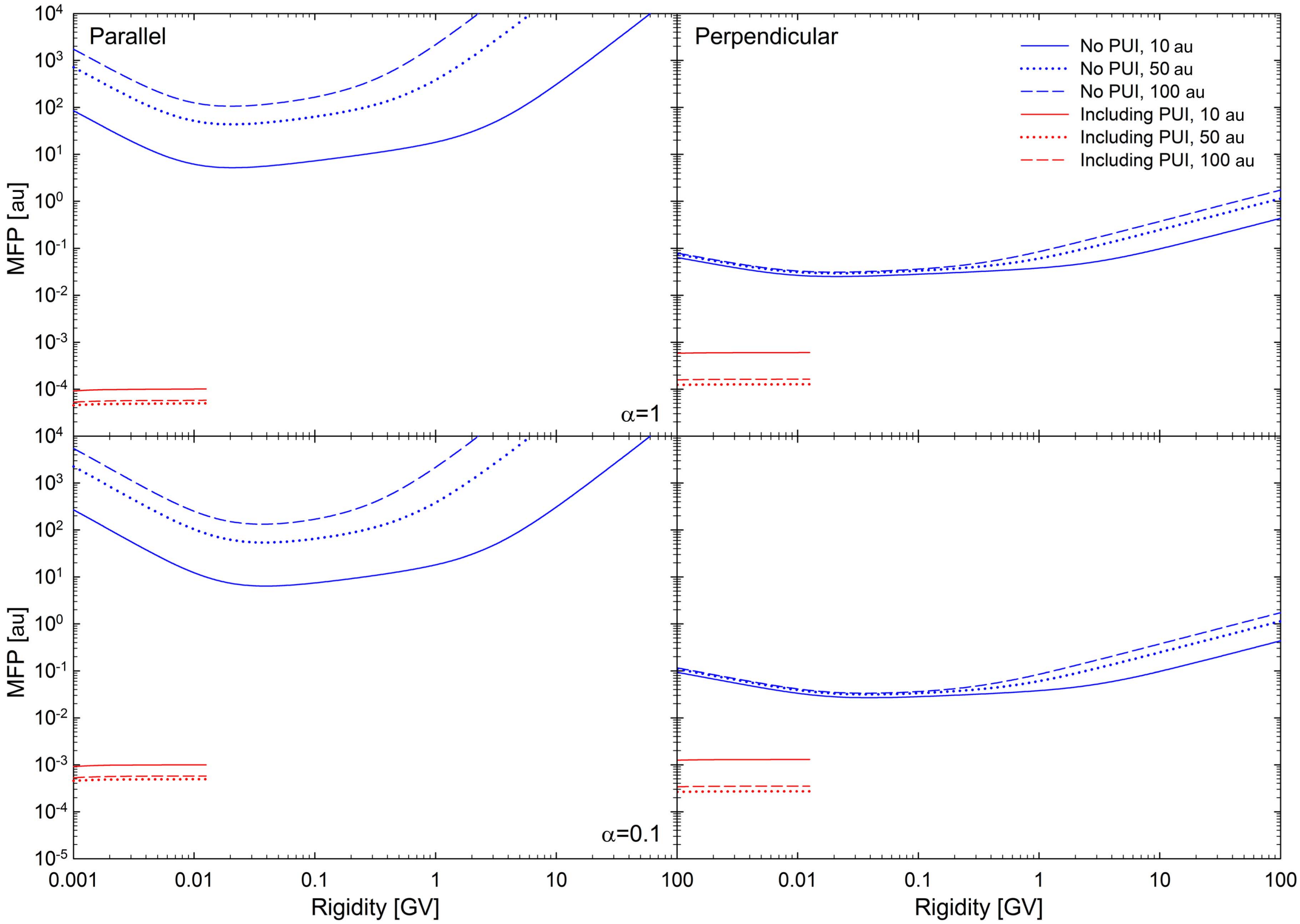

Figure 2. Parallel mean free paths at various radial distances taking into account PUI effects (red lines) and neglecting them (blue lines; Equation (6)), as a function of rigidity for full dynamical effects ($\alpha = 1$; top panels) and reduced dynamical effects ($\alpha = 0.1$; bottom panels).

so as to take into account an arbitrary ratio of slab to 2D energy. This is given by

$$\lambda_\perp = \left[\alpha_\perp^2 \sqrt{3\pi}\,\frac{2\nu - 1}{\nu}\frac{\Gamma(\nu)}{\Gamma(\nu - 1/2)}\lambda_{2D}\frac{\delta B_{2D}^2}{B_0^2}\right]^{2/3}\lambda_\parallel^{1/3}, \quad (10)$$

where it is assumed that $\alpha_\perp^2 = 1/3$ and $\nu = 5/6$ denotes half the assumed inertial range spectral index. Note that dynamical effects are neglected in the derivation of this expression. As v_A assumes very small values in the outer heliosphere, this should still provide reasonable values as to $\lambda_\perp$. It should also be noted that this expression is derived using a turbulence spectrum that has a flat energy-containing range, which is not entirely realistic (see Matthaeus et al. 2007), but which for the purposes of comparison has the benefit of having been used in previous electron modulation studies, as well as providing results not vastly different from those derived using a more realistic spectral form (Engelbrecht & Burger 2013a). Expressions for $\lambda_\perp$ derived using different energy-containing range spectral indices can be found in Shalchi et al. (2010) as well as Engelbrecht & Burger (2015). The results of this calculation are shown in the right panel of Figure 2. The solutions where PUI effects have been neglected are considerably smaller than the corresponding $\lambda_\parallel$ values, with a less steep rigidity dependence, in contrast with what is usually assumed in cosmic-ray modulation studies. A decrease in dynamical effects leads to larger perpendicular MFPs due to their dependence on $\lambda_\parallel$. When $\alpha = 1$, the PUI-affected solutions are very small relative to $\lambda_\perp$ when PUI effects are ignored, as expected, but now assume values larger than the corresponding parallel MFPs. This is a consequence of the $\lambda_\parallel^{1/3}$ dependence in Equation (10). Choosing $\alpha = 0.1$ leads to perpendicular MFPs smaller than the corresponding $\lambda_\parallel$ at 50 and 100 au, and larger at 10 au.

To study the effects of PUI-driven waves on the electron drift coefficients, an expression for the turbulence-reduced drift coefficient proposed by Engelbrecht et al. (2017) is employed, where the lengthscale corresponding to the drift coefficient is given by

$$\lambda_A = R_L\left[1 + \frac{\lambda_\perp^2}{R_L^2}\frac{\delta B_T^2}{B_0^2}\right]^{-1}, \quad (11)$$

where δB_T^2 denotes the total transverse variance. This expression reduces to the weak scattering, full drift lengthscale in the absence of turbulence. Figure 3 shows this drift lengthscale as function of rigidity for $\alpha = 1$ and $\alpha = 0.1$ at various radial distances, including the PUI-affected perpendicular MFPs from Figure 2 for the purposes of comparison.

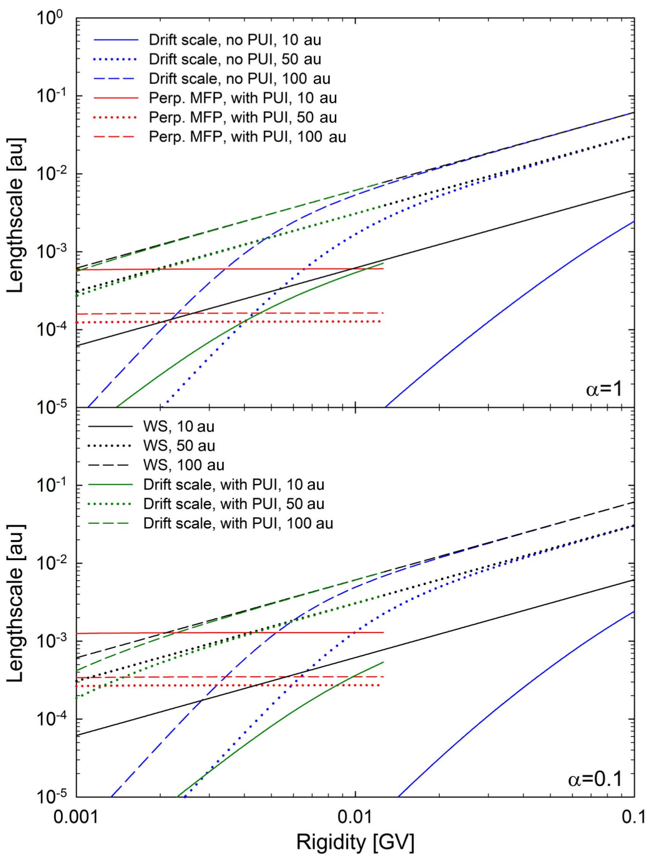

Figure 3. Drift scales at various radial distances taking into account PUI effects (green lines) and neglecting them (blue lines; Equation (6)), as a function of rigidity for full dynamical effects ($\alpha = 1$; top panels) and reduced dynamical effects ($\alpha = 0.1$; bottom panels). Weak scattering drift scales and PUI-affected perpendicular MFPs from Figure 2 are indicated with black and red lines, respectively. Note the difference in scales between this and Figure 2.

Note that this figure is plotted on a different scale to that of Figure 2, for the purpose of clarity. Solutions computed without PUI effects (blue lines) decrease sharply from the weak scattering values (black lines) at the lowest rigidities, due to the larger values of $\lambda_\perp$ at these rigidities, and remain well below the $\lambda_\perp$ calculated assuming no PUI effects for both values of α. When PUI effects are included, though, the drift lengthscale at 10 au also drops below the weak scattering value for both values of α, and remains below the corresponding $\lambda_\perp$. At 50 and 100 au, however, the PUI-influenced drift coefficient becomes very similar to the weak scattering values. This is a consequence of the very small values assumed by $\lambda_\perp$. At these radial distances, then, the drift scale actually becomes larger than $\lambda_\perp$ for both values of α considered here.

3. Discussion

When PUI effects are neglected, the resulting diffusion tensor is in reasonable agreement with what has long been assumed in previous modulation studies of low-energy electrons, with large parallel MFPs at the lowest energies and perpendicular MFPs much larger than the corresponding drift scales, in line with the idea that drift effects have little to no influence on low-energy electron transport (e.g., Ferreira et al. 2001a, 2001b). There are, however, differences in terms of, for example, the rigidity dependences of these quantities. The picture changes considerably when PUI effects are taken into account. In the extreme case of full dynamical effects, the MFPs shown in the top panels of Figure 2, including the effects of PUI-driven waves, are considerably lower in value than what has been expected from previous modulation studies (e.g., Ferreira et al. 2001a, 2001b; Zhang et al. 2007) and thus, by implication, could prove to be a significant barrier to Jovian electron transport beyond ∼10 au. Observational evidence from *Pioneer* 10, however, does not seem to support this, in that evidence for a predominantly Jovian component in electron intensities exists out to ∼25 au (Eraker 1982; Lopate 1991). *Voyager* data appear to support the *Pioneer* observations, but it has been noted that the *Voyager* observations of low-energy electrons at these energies could potentially be contaminated by proton interactions with the spacecraft frame that produce additional electrons (Potgieter & Nndanganeni 2013). Decreasing dynamical effects, however, lead to larger parallel and perpendicular MFPs and changes in their relative magnitudes, but these quantities remain considerably different to what has been used in previous modulation studies. Furthermore, including PUI effects leads to interesting consequences for the electron drift coefficients in that, in the outer heliosphere, these approach the weak scattering values, which are larger than the corresponding perpendicular MFPs. Overall then, the inclusion of PUI-driven waves in as self-consistent a manner as possible in the calculation of various low-energy electron transport coefficients leads to some highly unusual consequences for these quantities. Therefore, before firm conclusions can be drawn, the effects on electron transport of the MFP expressions and drift coefficients derived here should be investigated using an ab initio approach to modulation. This is imperative as, for instance, the large reduction in $\lambda_\parallel$ would have significant consequences for many modulation studies of Jovian and galactic electrons as well as positrons in the outer heliosphere (see, e.g., Strauss et al. 2011; Della Torre et al. 2012; Engelbrecht & Burger 2013b; Potgieter et al. 2015). Future work will also look into the effect these PUI-generated wave spectra would have on MFPs derived using different scattering theories, like the Weakly Nonlinear Theory (see Shalchi 2009) or the Unified Nonlinear Theory (e.g., Shalchi 2010).

N.E.E. would like to thank M. Venter, S. E. S. Ferreira, R. D. Strauss, and R. A. Burger in particular for many useful discussions.

ORCID iDs

N. Eugene Engelbrecht https://orcid.org/0000-0003-3659-7956

References

Aggarwal, P., Taylor, D. K., Smith, C. W., et al. 2016, ApJ, 822, 94
Bieber, J. W., Matthaeus, W. H., Smith, C. W., et al. 1994, ApJ, 420, 294
Breech, B. A., Matthaeus, W. H., Cranmer, S. R., Kasper, J. C., & Oughton, S. 2009, JGR, 114, A09103
Breech, B. A., Matthaeus, W. H., Minnie, J., et al. 2008, JGR, 113, A08105
Burger, R. A., Krüger, T. P. J., Hitge, M., & Engelbrecht, N. E. 2008, ApJ, 674, 511
Cannon, B. E., Smith, C. W., Isenberg, P. A., et al. 2014a, ApJ, 784, 150
Cannon, B. E., Smith, C. W., Isenberg, P. A., et al. 2014b, ApJ, 787, 133
Cannon, B. E., Smith, C. W., Isenberg, P. A., et al. 2017, ApJ, 840, 13
Della Torre, S., Bobik, P., Boschini, M. J., et al. 2012, AdSpR, 49, 1587
Earl, J. A. 1974, ApJ, 193, 231

Engelbrecht, N. E., & Burger, R. A. 2010, AdSpR, 45, 1015
Engelbrecht, N. E., & Burger, R. A. 2013a, ApJ, 772, 46
Engelbrecht, N. E., & Burger, R. A. 2013b, ApJ, 779, 158
Engelbrecht, N. E., & Burger, R. A. 2015, ApJ, 814, 152
Engelbrecht, N. E., Strauss, R. D., le Roux, J. A., & Burger, R. A. 2017, ApJ, 841, 107
Eraker, J. H. 1982, ApJ, 257, 862
Ferreira, S. E. S., Potgieter, M. S., Burger, R. A., et al. 2001a, JGR, 106, 29313
Ferreira, S. E. S., Potgieter, M. S., Burger, R. A., Heber, B., & Fichtner, H. 2001b, JGR, 106, 24979
Giacalone, J., & Jokipii, J. R. 1999, ApJ, 520, 204
Hellinger, P., & Trávníček, P. M. 2016, ApJ, 832, 32
Hunana, P., & Zank, G. P. 2010, ApJ, 718, 148
Isenberg, P. A. 2005, ApJ, 623, 502
Isenberg, P. A., Smith, C. W., Matthaeus, W. H., & Richardson, J. D. 2010, ApJ, 719, 716
Jokipii, J. R. 1966, ApJ, 146, 480
Joyce, C. J., Smith, C. W., Isenberg, P. A., Murphy, N., & Schwadron, N. A. 2010, ApJ, 724, 1256
Leamon, R. J., Matthaeus, W. H., Smith, C. W., Zank, G. P., & Mullan, D. J. 2000, ApJ, 537, 1054
Lee, M. A., & Ip, W. H. 1987, JGR, 92, 11041
Lopate, C. 1991, Proc. ICRC (Dublin), 2, 149
Matthaeus, W. H., Bieber, J. W., Ruffolo, D., Chuychai, P., & Minnie, J. 2007, ApJ, 667, 956
Matthaeus, W. H., Qin, G., Bieber, J. W., & Zank, G. P. 2003, ApJL, 590, L53
Oughton, S., Matthaeus, W. H., Smith, C. W., Bieber, J. W., & Isenberg, P. A. 2011, JGR, 116, A08105
Parker, E. N. 1958, ApJ, 128, 664
Potgieter, M. S., & Nndanganeni, R. R. 2013, Ap&SS, 345, 33
Potgieter, M. S., Vos, E. E., Munini, R., et al. 2015, ApJ, 810, 142
Richardson, J. D., Paularena, K. I., Lazarus, A. J., & Belcher, J. W. 1995, GeoRL, 22, 325
Scherer, K., Fichtner, H., Fahr, H.-J., Bzowski, M., & Ferreira, S. E. S. 2014, A&A, 563, A69
Schlickeiser, R. 2002, Cosmic Ray Astrophysics (Berlin: Springer)
Schwadron, N. A., & McComas, D. J. 2010, ApJL, 712, L157
Shalchi, A. 2009, Nonlinear Cosmic Ray Diffusion Theories (Berlin: Springer)
Shalchi, A. 2010, ApJL, 720, L127
Shalchi, A., Bieber, J. W., & Matthaeus, W. H. 2004, ApJ, 604, 675
Shalchi, A., Li, G., & Zank, G. P. 2010, Ap&SS, 325, 99
Simpson, J. A., Hamilton, D., Lentz, G., et al. 1974, Sci, 183, 306
Smith, W. S., Matthaeus, W. H., Zank, G. P., et al. 2001, JGR, 106, 8253
Strauss, R. D., Potgieter, M. S., Büsching, I., & Kopp, A. 2011, ApJ, 735, 83
Teufel, A., & Schlickeiser, R. 2003, A&A, 397, 15
Weygand, A. V., Goldstein, M. L., & Matthaeus, W. H. 2016, ApJ, 820, 17
Wiengarten, T., Oughton, S., Engelbrecht, N. E., et al. 2016, ApJ, 833, 17
Williams, L. L., & Zank, G. P. 1994, JGR, 99, 19229
Zank, G. P. 1999, SSRv, 89, 413
Zank, G. P., Adhikari, L., Hunana, P., et al. 2017, ApJ, 835, 147
Zhang, M., Qin, G., Rassoul, H., Lopate, C., & Heber, B. 2007, P&SS, 55, 12